

Comparison of Four Different Fluid Structure Interaction Models in a Human Coronary Artery

A. Javadzadegan¹, A.S.C. Yong², M. Chang², N. Mansour¹, M.K.C. Ng³, M. Behnia¹, L. Kritharides²

¹Department of Mechanical Engineering
The University of Sydney, Sydney, NSW 2006, Australia

²Department of Cardiology
Concord Hospital, The University of Sydney, Sydney, NSW 2139, Australia

³Department of Cardiology
Royal Prince Alfred Hospital, Sydney, NSW 2050, Australia

Abstract

Beside pulsatile motion of vessel, there are two additional movements of coronary arteries. One is from the pulsatile momentum of coronary artery while dampened by the supporting soft tissues. Another movement is responsible by contracting myocardium throughout the cardiac cycle with part of epicardial artery tethered to myocardium. In this study, four different external boundary conditions of vessel wall with different degree of rigidity are adapted in fluid-structure interaction (FSI) simulation with realistic geometry re-constructed from left anterior descending (LAD) coronary artery of a coronary angiogram. The results showed that degree of rigidity of the vessel markedly affects the magnitude of wall shear stress (WSS) and the length of recirculation flow in post stenotic regions, especially in the early diastole corresponding to the time of peak flow in coronary arteries.

1. Introduction

Coronary artery disease (CAD) is one of the leading causes of death in the world, claiming approximately 45% of cardiovascular deaths, which equates to 7.2 million deaths per year or 12% of deaths worldwide [3]. The primary disorder being atherosclerosis, leads to formations of blood clots resulting in heart and limb pain, which can then potentiate into heart attack and stroke. The coronary artery lies embedded on the surface of the heart. This anatomic location makes the vessel susceptible to the regular cardiac motion due to systolic and diastolic phases. The tethering of the artery to the external surface of the heart also restricts some movement.

Ways to mimic the coronary artery using computational fluid dynamics has improved significantly over time. Initial trials began by assuming the artery was a straight rigid tube [1, 2, 4]. Although initially progressive in the computational approach, this model does not consider the movement of the artery due to surrounding tissue and cardiac motion. *In-situ*, the vessel is affected by these surrounding factors. An approach into forming a model that mimics the physiological artery is of great importance for future work into this field. Since the rigid model does not accurately depict the true physiological artery, there have been numerous attempts at simulating the human artery in a realistic manner by investigating the extent and impact of vessel rigidity [5, 7, 8]. The realistic geometry of the model is also not considered in this approach. In reality the artery has a varying diameter. It is also not perfectly straight, rather having natural convolutions. To overcome this, more complex geometries were constructed in computer-aided drawing programs. It is now

possible to almost precisely reproduce a human artery through technologies such as intravascular ultrasound (IVUS) and magnetic resonance imaging (MRI).

The issue with much of previous literature is a way to account for all the physiological characteristics of an artery, and include them in a computational simulation. This study explores the best way to achieve this by investigating four different cases with different degree of rigidity. Each case has distinctive supports placed upon it. Determining the quantitative difference in parameters of interest (WSS and velocity streamline) for each case could aid prospective endeavours in the field.

2. Geometry and Material

2.1. Blood Model

Blood is assumed to be an incompressible, homogeneous and Newtonian fluid. The kinematic viscosity and density of blood are set to 0.0035 Pa s and 1050 kg/m³ respectively. Although blood is physiologically heterogeneous and therefore compressible, in simulations of large arteries the effects are negligible [6, 9].

2.2. Geometry

The model used in this study is based on a real patient with stenosis in the left anterior descending artery and its geometry were reconstructed using three-dimensional quantitative coronary angiography. The artery consists of a fluid and structural region. In Figure 1(a-c) the fluid domain, the structural domain and the integrated fluid and structural domains are shown. The regions are meshed using tetrahedral elements with a patch conforming method. The total number of elements varies from case to case, however the solid domain averages at 100000-150000 elements and the fluid domain ranges from 200000-300000 elements. The density of the artery wall is also considered to be 1050 kg m⁻³. Each artery has a Young's Modulus of 1 MPa and Poisson ratio of 0.3.

3. Boundary Conditions

The physiological proximal (P_a) and distal (P_d) arterial pressure measurements were performed using a pressure-temperature sensor guidewire. For steady conditions, the averaged proximal and distal pressures were set as the inlet and outlet boundary conditions respectively. The artery wall has a no slip boundary condition at the fluid-solid interface. For transient cases, the

time-dependant proximal and distal pressure profiles were used as the boundary conditions.

The four cases with their respective supports are demonstrated in Figure 1 (d-g) and are listed below. Each case was investigated using the patient-specific artery in the study.

3.1. Model (I)

The first support applied to each case is a rigid support. This has the affect of eliminating any movement of the artery, both inner and outer, due to blood dynamics.

3.2. Model (II)

This support restricts movement at the inlet and outlet in all degrees of freedom. The inner and outer wall is free to move due to internal haemodynamics.

3.3. Model (III)

This support allows movement of the artery in all places except the inlet. There is a fixed support on the inlet and a frictionless support at the outlet.

3.4. Model (IV)

In this model all movement is allowed at inlet, outlet, inner wall and outer wall. There are no added fixtures acting on the vessel.

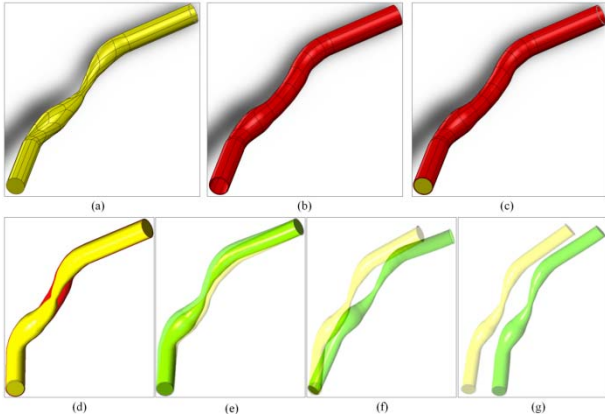


Figure 1. (a) Fluid domain, (b) Structural domain, (c) Integrated fluid and structural domains, (d) Model I, (e) Model II, (f) Model III, (g) Model IV

4. Numerical Method

For this study ANSYS and CFX (ANSYS CFX 12.1, Canonsburg, USA) were used to analyse the four artery cases. The solid domain is resolved using ANSYS, while the blood acting within the vessel is solved using the CFX (Fluid) feature. The high order backwards Euler algorithm is used. A time step of 0.01 s is used for the transient step in this study. Steady simulations for each case are then used as the respective initial conditions for the transient simulations.

The equations governing the fluid domain:

$$\frac{\partial u_i}{\partial x_i} = 0 \quad (1)$$

$$\frac{\partial u_i}{\partial t} + u_j \frac{\partial u_i}{\partial x_j} = \frac{1}{\rho_f} \frac{\partial p}{\partial x_i} + \frac{1}{\rho_f} \frac{\partial \tau_{ij}}{\partial x_j} \quad \text{in } {}^F\Omega(t) \quad (2)$$

where f is the fluid and p is the artery wall, u_i is velocity vector and p is the fluid pressure, ρ_f is the fluid density and τ_{ij} is the fluid stress tensor and ${}^F\Omega(t)$ is the moving spatial domain of the fluid.

The equations governing the solid domain:

$$\frac{\partial \sigma_{ij}}{\partial x_i} + f_i = \rho_p \frac{\partial u_i}{\partial t} \quad \text{in } {}^S\Omega(t) \quad (3)$$

$$\sigma_{ij} = D_{ijkl} \varepsilon_{kl} \quad \text{in } {}^S\Omega(t) \quad (4)$$

where ${}^S\Omega(t)$ is the spatial domain of the structure and σ_{ij} is the structure stress tensor, D_{ijkl} is the Lagrangian elasticity tensor and ε_{kl} is the structural strain tensor.

The coupling boundary condition:

$$\sigma_f \cdot n_f = \sigma_p \cdot n_p \quad (5)$$

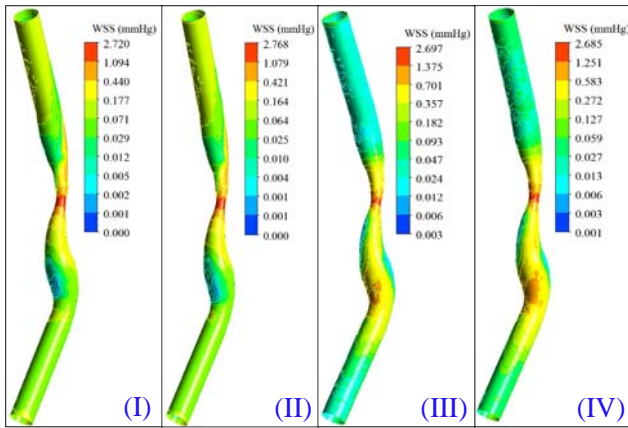
$$u_f = u_p \quad (6)$$

where σ , n and u are the stress tensor, normal vector and velocity vector of the fluid-structure interface respectively.

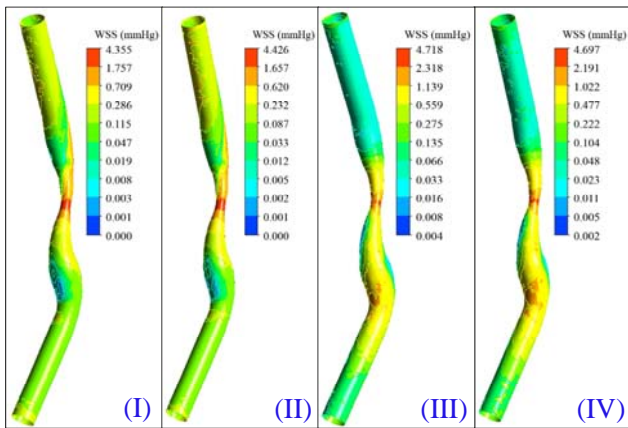
4. Results and Discussion

We performed transient simulations on the patient for each Model (I)-(IV). Contour plots (Figure 2) were constructed showing the WSS distribution for each Model at (a) the systolic phase, and (b) early diastolic phase, the time of the peak flow. It is clear that the systolic phase has a smaller WSS when compared to early diastole, as expected. During the event of diastole, both Models (I) and (II) show similar WSS contour distribution, with the point of stenosis in particular corresponding to a maximum WSS of 4.355 and 4.426 mmHg respectively. Models (III) and (IV) also show similar WSS contour plots, with the point of stenosis corresponding to a maximum WSS of 4.718 and 4.697 mmHg respectively. Models (III) and (IV) elicit a larger WSS at point of stenosis, perhaps due to the more liberal constraints applied to the artery, allowing for greater displacement. It is possible that Models (I) and (II) slightly under-exaggerate the WSS in areas of stenosis due to the degree of rigidity of the artery walls.

Direct comparison of time-averaged wall shear stress (WSS) of each Model using linear regression analysis was undertaken (Figure 3). Models (I) and (II) show near perfect correlation with an r^2 of 0.99 and slope (a) of 1. When comparing (I) vs. (III) and (I) vs. (IV), a weak correlation is found, with an r^2 of 0.33 for both. For both comparisons a slope of 0.55 was measured, suggesting Models (III) and (IV) show WSS approximately double to that of (I). Upon comparing (II) vs. (III) and (II) vs. (IV) similar correlations were observed. In the event of Model (III) vs. (IV) a perfect correlation is discovered with both an r^2 and slope of 1.0. The similarity between (I) and (II) is expected due to the similar constraints placed upon the artery. The same can be said of Models (III) and (IV), which have a similar freedom of movement, likely to account for the strong correlation in WSS distribution. The significant differences in (I) and (II) compared to (III) and (IV) also point to the suggestion that the degree of rigidity is the primary factor responsible for the difference in WSS values.



(a)



(b)

Figure 2. Wall shear stress (WSS) contour plot at (a) systolic phase and (b) early diastole, the time of peak flow.

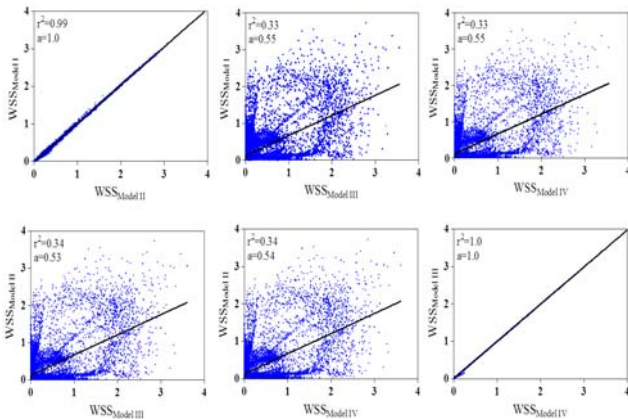


Figure 3. Correlations of time-averaged wall shear stress (WSS) between models. a and r^2 denote the gradient of the regression line and correlation coefficient.

Velocity streamlines (Figure 4) compare the extent of recirculation in each Model. At the point of stenosis, each Model shows different maximum velocities. Model (I) has the largest maximum velocity of 4.415 m/s, then in decreasing magnitude; Models (IV), (II) and lastly (III) with a velocity of 3.067 m/s. Areas of recirculation are substantially more evident in Models (III) and (IV) and seemingly absent in (I) and (II). The rigid-like constraints acting on the artery seem to reduce the recirculation present in the occluded coronary artery.

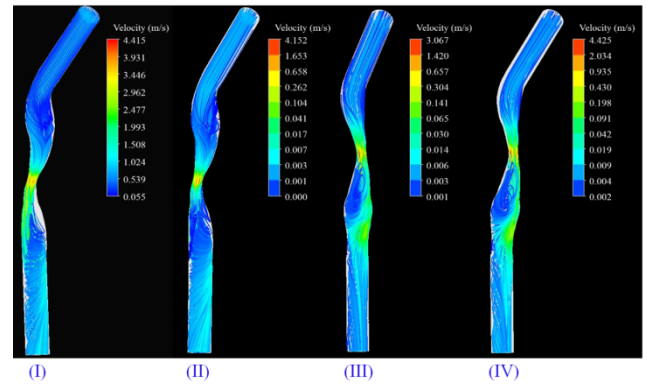


Figure 4. Velocity streamlines of Models (I) – (IV), showing the degree to which each model predicts backflow.

5. Conclusion

The rigidity of the vessel markedly affects the magnitude of WSS, especially in the diastolic phase. Models (III) and (IV), which allow for more artery movement results in higher WSS values. The effect of the constraints for each Model on the velocity of blood through the artery is especially noticeable in Models (III) and (IV). At the point of stenosis recirculation zones are more evident in these same Models, with a diminished effect via the restraints placed upon the artery with Models (I) and (II). Models (I) and (II) seem to reduce or dampen the magnitude and incidence of the haemodynamic parameters of interest. This is seemingly due to what they have in common; their relative rigidity. Models (III) and (IV) show more exaggerated values for WSS and velocity, most likely due to their freer range of movement.

6. References

- [1] Taylor, C. & Zairns T. H., C., Finite Element Modelling of Blood Flow in Arteries, *Computational Methods in Applied Mechanics and Engineering*, **158**, 1998, 155-196
- [2] Giulio Lorenzini, E. C., CFD analysis of pulsatile blood flow in an atherosclerotic human artery with eccentric plaques, *Journal of Biomechanics*, **41**, 2008, 1862–1870.
- [3] John F. Beltrame, R. D. a. R. T., *Coronary Artery Disease - Current Concepts in Epidemiology, Pathophysiology, Diagnostics and Treatment*. D. D. Gaze, InTech, 2012.
- [4] Pektold, K., Rappitsch, G., Loew, M., Kuban, B., Friedman, M., Validated Computation of Physiologic Flow in a Realistic Coronary Artery Branch, *Journal of Biomechanics*, **31**, 1998, 217-228.
- [5] Toloui, M. & Saidi, M.S., A numerical study of the effects of blood rheology and vessel deformability on the haemodynamics of carotid bifurcation, *Scientia Iranica*, **19**, 2011, 119-126.
- [6] Zhao, S.Z., Hughes, S.A., Thom, A.V., Stanton, B. & Long, Q., Blood flow and vessel mechanics in a physiologically realistic model of a human carotid arterial bifurcation, *Journal of Biomechanics*, **33**, 2000, 975-984.

[7] Siogkas, S. A., Exarchos, T. P., Stefanou, K., Fotiadis, D. I., Naka, K. K., Michalis, L. K., Filipovic, N. & Parodi, O., Blood flow in arterial segments: rigid vs. deformable walls simulations, *Journal of the Serbian Society for Computational Mechanics*, **5**, 2011, 69-77.

[8] Siogkas, P. K., Sakellarios, A. I., Stefanou, K. A., Exarchos, T. P., Tsakanikas, V. D., Michalis, L. K., Naka, K. K., Papafaklis, M. I., Bourantas, C. V. & Fotiadis, D. I., Blood flow in coronary arteries with deformable walls, *HSTAM International Congress on mechanics*, 2010.

[9] Wang, X. & Li, X., A fluid-structure interaction study on the biomechanical behaviour of a curved artery with flexible wall, *Journal of Medical Engineering & Technology*, **35**, 2011, 402-409.